Moisture Uptake in Nanocellulose: The Effect of Relative Humidity, Temperature and Degree of Crystallinity

Mohit Garg
Laboratory of Organic Electronics, Linkoping University https://orcid.org/0000-0001-6563-3106
Varvara Apostolopoulou-Kalkavoura
Stockholms Universitet
Mathieu Linares
Linkopings universitet
Tahani Kaldéus
KTH Royal Institute of Technology
Eva Malmström
KTH Royal Institute of Technology: Kungliga Tekniska Hogskolan
Lennart Bergström
Stockholm University: Stockholms Universitet
Igor Zozoulenko (igor.zozoulenko@liu.se)
Linkopings universitet

Research Article

Keywords: Moisture Uptake, Humidity, Temperature, Degree of Crystallinity

Posted Date: February 12th, 2021

DOI: https://doi.org/10.21203/rs.3.rs-188647/v1

Version of Record: A version of this preprint was published at Cellulose on July 29th, 2021. See the published version at https://doi.org/10.1007/s10570-021-04099-9.

Abstract

Foams made from cellulose nanomaterials are highly porous and possess excellent mechanical and thermal insulation properties. However, the moisture uptake and hygroscopic properties of these materials need to be better understood for their use in biomedical and bioelectronics applications, in humidity sensing and thermal insulation. In this work, we present a combination of hybrid Grand Canonical Monte Carlo and Molecular Dynamics simulations and experimental measurements to investigate the moisture uptake within nanocellulose foams. To explore the effect of surface modification on moisture uptake we used two types of celluloses, namely TEMPO-oxidized cellulose nanofibrils and carboxymethylated cellulose nanofibrils. We find that the moisture uptake in both the cellulose nanomaterials increases with increasing relative humidity (RH) and decreases with increasing temperature, which is explained using the basic thermodynamic principles. The measured and calculated moisture uptake in amorphous cellulose (for a given RH or temperature) is higher as compared to crystalline cellulose with TEMPO- and CM-modified surfaces. The high water uptake of amorphous cellulose films is related to the formation of water-filled pores with increasing RH. The microscopic insight of water uptake in nanocellulose provided in this study can assist the design and fabrication of high-performance cellulose materials with improved properties for thermal insulation in humid climates or packaging of water sensitive goods.

1. Introduction

Cellulose is one of the most abundant biopolymers on Earth. It can be found in wood, algae, tunicates, and cotton usually combined with other components such as hemicellulose and lignin.(Cosgrove 2005) Cellulose is a light-weight and versatile material that exhibits a structural hierarchy from the ångstrom- to the micrometer scale, and cellulose nanomaterials (CNM) display a high surface area and tunable surface chemistry making them versatile materials for a variety of applications.(Klemm et al. 2011; Moon et al. 2011; Thomas et al. 2018) CNM in the form of cellulose nanocrystals (CNC) or cellulose nanofibrils (CNF) can be produced by acid hydrolysis or mechanical and chemical defibrillation, respectively. (Phanthong et al. 2018) Sulfuric acid hydrolysis or the chemical modification (i.e., TEMPO mediated oxidation or carboxymethylation) replaces the primary hydroxyl group (-OH) on cellulose surface by common functional groups such as sulfate ($-OSO_3^-$), carboxylate ($-COO^-$) and carboxymethyl ($-CH_2COO^-$). (Saito and Isogai 2004; Liimatainen et al. 2013; Eyley and Thielemans 2014; Candido and Gonçalves 2016; Kaldéus et al. 2018)

CNFs and CNCs have been extensively used to make thin films(Lavoine and Bergström 2017; Kontturi and Spirk 2019), foams and aerogels(Lavoine and Bergström 2017; Kontturi and Spirk 2019) for a wide range of applications including e.g., packaging(Trache et al. 2016), photonics,(Shrestha et al. 2017; Chen et al. 2020) thermal insulation,(Antonini et al. 2019) pharmaceuticals,(Picheth et al. 2017) and membranes.(Li et al. 2019) CNM-based materials often display excellent mechanical, optical, barrier, and heat insulation properties.(Lavoine and Bergström 2017; Hamad 2017; Parker et al. 2018) However, cellulose is naturally hygroscopic, i.e., its properties change drastically when exposed to a humid environment due to the

presence of hydroxyl groups on the surface. Indeed, the moisture content in wood, which consists mainly of cellulose, lignin, hemicellulose and extractives, can vary from 10% to 40% depending on the relative humidity (RH), where RH at a given temperature is defined as the ratio of partial pressure of vapor to the vapor pressure of water. Interestingly, the moisture uptake depends also on functionalization of cellulose. For example, TEMPO-oxidized cellulose nanofibrils adsorb more moisture compared to the sulfated cellulose nanofibrils at a RH of 95%.(Guo et al. 2018) Furthermore, there are numerous studies that have showed that the strength, toughness and Young's modulus of cellulosic films are significantly reduced with increasing RH(Benítez et al. 2013; Benítez and Walther 2017) and that the fiber-matrix adhesion can be reduced by moisture uptake.(Haslach 2000; Mokhothu and John 2015) Moisture uptake by packaging materials for the pharmaceutical industry can also cause stability problems for moisture sensitive drugs.(Mihranyan et al. 2004) However, the quick and sensitive response of cellulose towards moisture can be used in humidity sensors following the change in gravimetric or viscoelastic properties due to water uptake.(Solin et al. 2020) Similarly, humidity-responsive chiral nematic CNC films utilize the increase in the chiral nematic pitch of the helix with uptake of water to the change of color of the film.(Chen et al. 2020) Recently, it was also shown that moisture-induced swelling of CNM-based foams can also reduce the thermal conductivity due to enhanced phonon scattering(Apostolopoulou-Kalkavoura et al. 2021).

The water uptake in cellulose is a microscopic phenomenon that can be captured by atomistic modelling. The moisture uptake in cellulose depends on several factors such as the cellulose-cellulose, cellulose-water and cellulose-counterion interactions which are governed by van der Waals and Coulombic interactions. The hydration of cellulose and the bound water inside the cellulose were studied using molecular dynamics (MD) simulation.(Garg et al. 2020) However, to investigate the effect of the RH on the moisture uptake inside the porous material the Grand Canonical Monte Carlo (GCMC) simulations are required. This is because the GCMC simulations allow the number of atoms in the system to fluctuate, which is needed to describe the case when water molecules are absorbed. Note that the GCMC simulations possess the drawback of constant volume meaning that the structure of cellulose does not change during the GCMC steps. However, the water uptake in cellulose is accompanied by structural changes and increase in pore volume. This cannot be captured by GCMC simulations alone and thus requires MD simulations as well.(Kulasinski et al. 2015; Chen et al. 2018)

To design and fabricate high-performance biopolymer-based materials, the mechanism of moisture uptake must be well understood in order to utilize these materials efficiently in various applications. For instance, the moisture uptake in chitosan films decreases with increasing temperature.(Aguirre-Loredo et al. 2017) The presence of surface charge and counterions seems to influence the sorption behavior of cellulose indicating that moisture sorption in sulfated cellulose is higher with H^+ and Na^+ counterion as compared to Ca^{2+} counterion.(Berthold et al. 1994) However, even if it is known that crystallinity, surface modification and temperature are crucial parameters affecting the moisture uptake of cellulose and CNMs(Kulasinski et al. 2015; Kulasinski 2016), their effect is not fully explored and remains not well understood.

Here we combined a hybrid Grand Canonical Monte Carlo/Molecular Dynamics simulations (GCMC/MD) with gravimetric moisture experiments to investigate the effect of temperature and the degree of crystallinity on moisture uptake of nanocellulose. The experimental measurements were performed on CNM foams prepared from CNC and CNF with different surface modifications and the simulations were performed on amorphous cellulose films and crystalline bundles with corresponding surface modifications. The moisture uptake was calculated at temperatures between 285 and 313 K and RH between 20 and 80%. The calculated data were correlated to various microscopical properties such as the radial distribution functions and the pore size distribution to understand the microscopic mechanism of moisture uptake.

2. Materials And Methods

Materials

A never-dried sulfite softwood cellulose pulp (Domsjö dissolving Plus) was provided by Domsjö Fabriker AB (Aditya Birla Domsjö, Sweden) and used as starting material. NaClO (Alfa Aesar), 2,2,6,6-tetramethyl-1-piperidinyloxy free radical (TEMPO, ≥ 98%, Alfa Aesar), sodium hydroxide (NaOH, P99.2%, VWR Chemicals), sodium bromide (NaBr, BioUltra, P99.5%, Sigma Aldrich) and sodium borohydride ($NaBH_4$, ≥ 98%, Sigma–Aldrich) were used as received.

The TEMPO-oxidized cellulose nanofibers (TCNF) were prepared as previously reported using the TEMPO/NaBr/NaClO system with 10 mmol of NaClO per gram of cellulose(Saito and Isogai 2004). The TEMPO-mediated oxidation was performed at pH 10 for 4 hours. The residual aldehyde and ketone groups in the TEMPO-oxidized cellulose pulp were reduced by adding 0.1 g of $NaBH_4$ per gram of cellulose to the pulp suspension at pH 10 and allowing it to stir for 3 h(Saito and Isogai 2006). The TEMPO-oxidized cellulose pulp obtained was washed thoroughly with deionized water (DI) to remove the excess reagents. The final TCNF material was obtained by grinding the TEMPO-oxidized cellulose pulp using a supermass colloider grinder (Model MKZA10-15J, Masuko Sangyo Co., Ltd, Japan) equipped with non-porous grinding stones containing silicon carbide (Disk model MKE), using a gap clearance of -100 µm at a motor frequency of 30 Hz.

The TEMPO-oxidized CNCs (TCNC) were obtained from TCNFs prepared with 10 mmol/g of NaClO. The TCNCs were obtained by HCl (2.5 M) acid hydrolysis of the TCNF for 4 h at 105 °C(Tanaka et al. 2015) as previously reported following by centrifugation and dialysis (DI water) to thoroughly clean the final material.

The carboxymethylated cellulose nanofibers (CMCNF) were prepared following the procedure reported before(Wågberg et al. 2008; Kaldéus et al. 2018). In short, cellulose fibers were solvent exchanged to ethanol whereafter the CNFs were impregnated by monochloroacetic acid in isopropanol. The cellulose fibers were then placed in an alkaline (NaOH) alcoholic solution (MeOH and iso-PrOH) at 82 °C. The carboxymethylation was conducted for 60 minutes whereafter work-up was conducted by filtration (DI

water, acetic acid (0.1 M), and DI water). To convert the pulp into the Na+ form, the CMCNFs were immersed in $NaHCO_3$-solution (4 wt%) and post-filtered with DI water. Finally, the carboxymethylated pulp was mechanically disintegrated in a high pressure microfluidizer (M-110EH, Microfluidics) by a single pass through the 400 µm and 200 µm chambers and four times through the 200 µm and 100 µm chambers following by sonication and centrifugation.

Preparation of Anisotropic CNM Foams

Anisotropic TCNF, TCNC and CMCNF foams were prepared by unidirectional ice templating(Wicklein et al. 2015; Munier et al. 2016) from 0.5wt% dispersions 0.5 wt% in DI. The unidirectional ice-templating was performed using teflon molds of 4 cm diameter and 2.5 cm height equipped with copper bottom plate that were filled with TCNF, TCNC or CMCNF dispersion and placed in contact with a dry ice block, giving a final cooling rate of 3 K min^{-1}. The final dry foams were obtained by removing the ice by sublimation at 0.024 mbar and room temperature for four days using a freeze-dryer (Christ Alpha 1-2LDplus, Germany).

CNM particles and CNM Foams Characterization

AFM (Dimension 3100, Bruker, USA) operated in tapping mode was used to determine the CNM dimensions (Figure S1). A droplet of 0.001-0.005 wt% aqueous CNM dispersion was deposited onto freshly cleaved mica substrate and dried at ambient conditions.

Conductometric titration(Committee 2002) with NaOH as titrant was used to determine the surface charge of CNMs to be 1.60 mmol COO^- per gram of cellulose for the TCNF and TCNC, and 0.65 mmol COO^- per gram of cellulose for the CMCNF.

SEM images of the CNM foams cross-section were taken using a HITACHI TM-3000 (Germany) using a 5 kV electron beam at a magnification of ×500.

The apparent density, ρ, of the foams was calculated from the mass and the volume (height x πr^2) of the foams, kept for 3 d at 50% *RH* and 295 K.

The porosity (Π) of the foams was determined from the skeletal (ρ_{skel})(Wicklein et al. 2015) and the apparent foam density (ρ_{app}).

The crystallinity index (CI) of the CNM foams was calculated from 1D diffractograms obtained with a Panalytical X'Pert PRO diffractometer operated with Cu Kα radiation and in Bragg-Brentano diffraction geometry. Thin pressed CNM foam samples (<1 mm) were mounted on a Si wafer zero-background holder spinning at a constant rate of 30 rpm and diffraction patterns were measured for 2θ between 5 and 50° with 0.0167° step size.

The CI was then calculated using the Segal method(Segal et al. 1959) (Equation 1).

$$CI(\%) = \frac{I_{200} - I_{am}}{I_{200}} \times 100 \quad (1)$$

where, I_{200} and I_{am} are the intensity values for the (200) peak of crystalline cellulose located at 2θ = 22-23° and the peak for amorphous cellulose located at 2θ = 18-19°, respectively. The angular values were measured with a copper (Cu) X-ray source.

Gravimetric Moisture Uptake

The moisture uptake of the CNM foams under controlled *RH* and temperature was determined gravimetrically by measuring the weight change using a high-precision balance (BP 210 S, Sartorius, Germany) placed inside a humidity chamber as described previously(Apostolopoulou-Kalkavoura et al. 2018). Prior to the measurements, the foams were dried at 313 K and 20 % *RH*. Further drying does not reduce the amount of water in the CNM foams, and therefore the material at this condition is considered as nominally dry. The moisture content on dry weight (w) basis, H_2O_w, (i.e., the weight of water divided by the weight of dry cellulose) as a function of *RH* (20, 35, 50, 65 and 80%) was assessed at 285, 295, 303, 308 and 313 K. Each measurement at a specific temperature and RH lasted six hours to ensure that steady state was reached, and the foam mass was measured every five minutes.

Computational Model

The amorphous and crystalline cellulose were modeled in the present work. The model of amorphous cellulose includes TEMPO-oxidized (TEMPO) amorphous cellulose and carboxymethylated (CM) amorphous cellulose. The cellulose chains with both the functionalities are shown in Figure 1(a-b). Similarly, the model of crystalline cellulose contains TEMPO-crystalline cellulose and CM crystalline cellulose. The degree of substitution was 1.6 mmol COO^-/g of cellulose and 0.6 mmol CH_2COO^-/g of cellulose for TEMPO- and CM-cellulose respectively (both amorphous and nanocrystalline cellulose). The Na^+ is used as the counter ion to make the system charge neutral.

The amorphous cellulose chains were generated with Avogadro.(Hanwell et al. 2012) The computational box with 16 cellulose chains containing 5 repeating cellobiose was generated with an initial density of 1 gm/cm^3. To generate the amorphous film, we followed the thermal annealing protocol where the film is first heated above the glass transition temperature of polymer and then quenched to the desired temperature. First the cellulose chains were equilibrated at a high temperature of 800 K in the NPT (constant number of particles, pressure, and temperature) ensemble with Nosé-Hoover thermostat and barostat with a coupling constant of 0.1 and 1 ps respectively. After equilibration at high temperature the amorphous film was quenched from 800 K to desired temperatures of 285 K, 295 K and 313 K at a cooling rate of 0.1 K/ps. The films were then equilibrated at these temperatures. The total time for equilibration was 10 ns and the final density of the film converged to 1.3 g/cm^3. Figure 3(c) shows a snapshot of amorphous film prepared using the above-mentioned procedure.

The crystalline cellulose consists of a cellulose nanocrystal (CNC) of dimensions 2.3×2.3×11 nm^3. The cellulose chains within the fibril were arranged in a square lattice with I_β crystal structure. Each fibril consists of 16 chains of cellulose with 5 repeating cellobiose units. Four CNCs were used, and they were arranged in a form of a bundle having a square cross section, see Figure 2(d). Note that the periodic boundary conditions are used, such that this arrangement corresponds to an infinite periodic structure. In order to make a dry film of CNCs bundle we run a short NPT simulation (constant number of particles, pressure, and temperature) in vacuum to form a bundle. The initial and final configuration of the CNCs in the bundle arrangement is illustrated in Figure 2(d). This approach was chosen to create a parallel arrangement of the CNCs with respect to each other as it is done in the experiments.

SimulationDetails

All simulations were run in LAMMPS molecular dynamics simulation software.(Plimpton 1995) The OPLS-AA force field parameters for cellulose was used for describing bonded and non-bonded interactions and were generated using the Maestro software suit of Schrödinger software.(Schrödinger 2018) The TIP3P water model is used for sorption.(Mark and Nilsson 2001) The water molecules were made rigid by using rigid body command in LAMMPS. The Ewald summation method was used for the long-range electrostatic interactions. The moisture uptake was measured by running hybrid Grand Canonical Monte Carlo (GCMC) and Molecular Dynamics (MD) simulations.(Plimpton 1995) The GCMC simulation allows the insertion/deletion of atoms at a constant volume and a specific chemical potential and MD simulation allows the relaxation of the system at constant stress. In this way the GCMC/MD approach allows the water intake in a static structure followed by a structural relaxation. The simulations at a specific temperature were performed by running both MD and GCMC steps. Each simulation window consists of running 100 MD steps followed by 1000 GCMC steps. The MD simulations were run in NσT (constant number of particles, stress, and temperature) ensemble with Nosé-Hoover thermostat and a constant stress of 0 Pa was maintained by Nosé-Hoover barostat. The time step for MD simulations was 1 fs. This was then followed by GCMC steps. The GCMC simulations were run in μVT (constant chemical potential, volume, and temperature) ensemble, where the water molecules can be adsorbed or desorbed from the cellulose at a specific chemical potential. To equilibrate the system using hybrid GCMC/MD simulations 10^5 windows of coupled GCMC/MD steps were run, which corresponds to a total time of 10 ns for each simulation.

Pore size calculations

A size of a pore at any point inside the material is defined as the maximal size of a sphere that can be fitted at that point without an overlap with other atoms. To calculate the pore size first we remove the water from the system. After that pore size inside the cellulose film is calculated using Zeo++ code. (Pinheiro et al. 2013) For all the calculations, the probe diameter of 1 Å was used.

3. Results And Discussion

Three different types of CNM foams were produced by ice-templating of 0.5 wt% TCNF, TCNC and CMCNF aqueous suspensions in a mold equipped with a copper bottom and teflon walls to allow unidirectional freezing. Interestingly, the surface charge density of the TCNF fibrils and the TCNC rods is identical although the different CNMs had quite different crystallinity indexes (CI=51 and 68 respectively) and aspect ratio (202 and 89, respectively) (Table 1). On the other hand, the CMCNF possess a lower surface charge density than TCNF and TCNC but a similar particle diameter and CI as the TCNF. The foam densities were similar for all foam types with the TCNC foams having a slightly higher densities due to their higher fragility. The water uptake was determined after conditioning the anisotropic CNM foams for 6 hours at 285, 295, 303, 308 and 313 K and 20-80% RH(Apostolopoulou-Kalkavoura et al. 2018).

Table 1. Characterization of the CNM particles and foams.

	Surface Groups	Surface Charge (mmol COO^- /g)	Particle Diameter (nm)	Aspect Ratio	Crystallinity Index (CI)	Foam ρ_{dry} (kg m^{-3})
1. TCNF	$-COO^-$	1.60 ± 0.01	2.3 ± 0.7	202 ± 16	51.1	5.9 ± 0.2
2. TCNC	$-COO^-$	1.60 ± 0.01	4.5 ± 1.3	89 ± 36	67.8	7.7 ± 0.3
3. CMCNF	$-CH_2COO^-$	0.65 ± 0.00	3.0 ± 0.6	N/A	45.8	6.3 ± 0.2

The effect of RH and temperature on the water uptake was also determined computationally by hybrid GCMC/MD simulations on bundles of 100% crystalline CNC (Fig. 2d), and amorphous cellulose films (Fig. 2c) with different surface modifications. The RH depends on the vapor pressure (P) at a specific temperature which in turn is related to the chemical potential. The RH is equal to P/P_0, with P_0 being the saturation vapor pressure. The saturation pressure of water at 285 K, 295 K and 313 K is 1200 Pa, 2300 Pa and 7000 Pa respectively. At these temperatures, the water vapor is assumed to be ideal gas with chemical potential (μ) according to Equation 2.

$$\mu - \mu_0 = k_B T \ln \mathrm{RH}, \qquad (2)$$

where μ_0 is the chemical potential of water at saturation vapor pressure, T is the temperature and k_B is the Boltzmann constant. Figure 3(c-d) present snapshots of the initial and final configurations of both amorphous and crystalline celluloses at 80% RH and temperature of 285 K. For the case of the amorphous cellulose (Figure 3c) the water molecules (blue beads) are adsorbed in the porous structure of cellulose causing geometrical swelling. For the case of the crystalline cellulose (Figure 3d) the water is not sorbed inside the nanocrystal because of the stacking of the cellulose chains that makes it naturally

hydrophobic and impenetrable for water. However, the water is adsorbed at the interface between the cellulose nanorods in the bundle, which causes a swelling of the film.

The calculated and measured moisture uptake as function of relative humidity is shown in Figure 3 for both TEMPO oxidized and carboxymethylated CNM foams with varying crystallinity as a function of RH and at different temperatures. The amorphous cellulose (CI=0) and crystalline cellulose (CI=100) were studied in simulation, whereas in the experimentally studied samples the crystallinity varied between CI=46 and 68 as specified in Table 1. The simulated and measured dependencies are consistent with each other and show the expected behavior as a function of the RH and temperature as prescribed by Eq. (2). Namely, as the RH increases the moisture uptake in cellulose increases due to the increase of the chemical potential of water according to Eq. (2). At the same time, at a given RH, as the temperature increases the moisture sorption decreases because of the decrease in the chemical potential of water according to Eq. 2. (Note that in Eq. 2, ln RH < 0).

The calculated moisture uptake in amorphous cellulose (for a given RH or temperature) is higher as compared to the crystalline cellulose for both TEMPO- and CM-modified surfaces, see Figures 3 a, b; and e and f. The experimental measurements for TEMPO-modified cellulose show the same trend where the moisture uptake (for a given RH or temperature) is higher for more amorphous material, i.e., for TCNF with CI=51.1 as compared to TCNF with CI=67.8, see Figure 4 cd. (Note that experimental measurements for CMCNF are available only for one degree of crystallinity). It is noteworthy that the higher water uptake on less crystalline CNMs corresponds well to previous work by Kulasinski et al. (Kulasinski et al. 2015; Kulasinski 2016) The CMCNF foams exhibit a slightly lower moisture uptake compared to the TCNF foams. However, a direct comparison for carboxymethylated and TEMPO oxidized celluloses cannot be made because of the lower degree of surface modification in the CMCNF compared to the TCNF.

Let us now compare quantitatively the experimental and simulated results. For lower temperatures of T=285K, 295K the moisture uptake at a temperature of for both TCNF and TCNC lies in between the corresponding simulated results for the amorphous and crystalline cellulose, c.f. Figures 4 cd and ab. The same also applies for CMCNF for the case of lower temperature T=295K, c.f. Figure 4 e, f and g. This is expected because the crystallinity CI of the experimental measured materials is in between of the one of completely amorphous and completely crystalline materials that were simulated numerically. However, at higher temperatures the moisture uptake in the experiment is lower compared to the simulations. We attribute this to the presence of the bounded water in experimental samples,(Niinivaara et al. 2015; Paajanen et al. 2019; Garg et al. 2020) which is difficult to remove even for elevated temperatures above 450 K.(Langan et al. 2014) This means that, in contrast to the simulations, in the experimental samples the relative humidity inside the material can be different in comparison to the one maintained in the chamber.

To obtain an insight of the moisture uptake on an atomistic level, let us investigate the changes in the morphology of the cellulose when the temperature changes. In what follows, we present results for the case of TEMPO-oxidized cellulose only. CM-modified cellulose shows a similar behavior, and the

corresponding results are presented in SI (Figure S1). Figures 4 a and c show the calculated pore size distribution for different temperatures for respectively TEMPO-amorphous and TEMPO-crystalline cellulose. A comparison of these distributions clearly shows that, as expected, pores are larger in the amorphous cellulose films compared to crystalline bundles. (Note that this can also be seen in the morphology snapshots presented in Figure 2 c, d). In addition, for the case of the crystalline cellulose the pore size distribution practically does not change when the temperature is varied. This can be explained by the rigidity of the crystalline structure of nanocellulose. In contrast, for the case of amorphous cellulose (which is less rigid and more structurally flexible), the pore size increases when the temperature decreases (i.e. when the water intake increases). Hence, because of the larger pore size in the amorphous cellulose, and because water is able to fill in additional pores that are created during water intake, the amorphous cellulose films absorb more water compared to the crystalline bundles.

It is noteworthy that the slopes of the simulated water intake dependencies as a function of RH are steeper for the amorphous cellulose as compared to the crystalline one (c.f. Figures 3 and b; Figure 3 e and f). Because of the formation of new pores for the case of the amorphous cellulose, it is expected that the corresponding slope is steeper, which is fully consistent with the simulated results.

Figures 4 b and d show the calculated radial distribution functions ($g_{O^-\text{-}OW}(r)$) between the oxygen (O^-) of carboxyl group in cellulose and oxygen (OW) of water for respectively TEMPO-amorphous and TEMPO-crystalline cellulose. (Note that the distribution functions $g_{O^-\text{-}OW}(r)$ defines the probability to find the oxygen (O^-) of carboxyl group in cellulose and oxygen (OW) of water separated by the distance r). The distribution functions exhibit a pronounced peak at $r \approx 3$Å signifying a formation of the hydration shells around the oxygen in the carboxyl group. The evolution of $g_{O^-\text{-}OW}(r)$ with temperature is strikingly different for the amorphous and crystalline cellulose and is fully consistent with the evolution of the pore size distribution discussed above. Namely, for the case of the amorphous structure the peak practically does not change with temperature (and thus with the water content), which means that the number of water molecules surrounding the oxygen in the carboxyl group remains the same. This is because in this case water molecules fill in additional pores that are formed during water intake. In contrast, no additional pores are created in the case of crystalline cellulose. As a result, the number of absorbed water molecules between the nanocrystals in the bundle increases, which is reflected in the increase of the peak of the distribution function $g_{O^-\text{-}OW}(r)$ as the temperature drops (i.e., when water content increases).

Note that above we presented the analysis of the pore size evolution with the change of the temperature. We also performed a similar analysis of the case when the RH changes. As discussed above (Figure 3 and related discussion in the text), the increase of the RH leads to same effect of the increase of the water intake as the decrease of the temperature. Therefore, as expected, the evolution of the pore size distribution and the changes in the distribution function $g_{O^-\text{-}OW}(r)$ with the change of RH exhibit very similar behavior as the one discussed above, see Figure S2.

Conclusions

In this study, we investigated the moisture uptake in cellulose nanomaterial foams using a combination of the hybrid Grand Canonical Monte Carlo and Molecular Dynamics simulations for TEMPO-oxidized or carboxymethylated amorphous and crystalline cellulose films and experimental measurements on foams made by TEMPO-oxidized cellulose nanofibrils (TCNF) and nanocrystals (TCNC) and carboxymethylated cellulose nanofibrils (CMCNF). The TCNF and TCNC exhibited the same surface chemistry allowing us to investigate the effect of varying crystallinity on the moisture uptake. The CMCNF fibrils having different surface chemistry but similar particle diameter and crystallinity with TCNF provide useful insight of the surface chemistry effect on the moisture uptake.

Both experiments and simulations show that the moisture uptake is enhanced when the relative humidity (RH) is increased, or when the temperature is decreased. This behavior is explained by the basic thermodynamics (Eq. (2)) governing the change of the chemical potential of water as a function of the temperature and the RH. Overall, the experimental moisture uptake in all studied materials is in good agreement with the simulations, especially at lower temperatures (T=285-295K). At higher temperatures (T=313K) the moisture uptake in experiments is lower compared to simulations. We attribute this to the presence of the bound water in experimental samples that is difficult to remove. TCNF and CMCNF exhibit a similar moisture uptake as a function of temperature and RH, both in experiments and in simulations.

We find, both experimentally and by simulations, that the water uptake in amorphous cellulose (for a given RH or temperature) is higher as compared to the crystalline cellulose for both TEMPO- and CM-modified surfaces. We related this to the difference in the structure and evolution of the pores in these materials. Namely, in the amorphous cellulose pores are larger, and more pores are formed during moisture uptake, allowing water to fill in these additional pores.

We hope that the microscopic understanding of the mechanism of water uptake provided in this study will pave the way to prepare high-performance cellulose materials with improved properties for selected applications such as thermal insulation in humid climates or transportation of moisture sensitive goods.

Declarations

Acknowledgements

L.B. acknowledges support from the Swedish Energy Agency (Energimyndigheten, project 2019-006749), and Formas (project 2015-2032), E.M., L.B., T. K, and I.Z acknowledges support from the Wallenberg Wood Science Center (WWSC). I.Z. acknowledges support of the Swedish Research Council (project 2016-05990), Tröedssons foundation and Åforsk. M.L. acknowledges support from the Swedish e-Research Centre (SeRC). The computations were performed on resources provided by the Swedish National Infrastructure for Computing (SNIC) at NSC and HPC2N.

Compliance with ethical standards

Conflict of interest

The authors declare that they have no conflict of interest.

Human and animal rights

This article does not contain any studies with human participants or animals performed by any of the authors.

References

Aguirre-Loredo RY, Rodriguez-Hernandez AI, Velazquez G (2017) Modelling the effect of temperature on the water sorption isotherms of chitosan films. Food Sci Technol 37:112–118. https://doi.org/10.1590/1678-457X.09416

Antonini C, Wu T, Zimmermann T, et al (2019) Ultra-porous nanocellulose foams: A facile and scalable fabrication approach. Nanomaterials 9:1–14. https://doi.org/10.3390/nano9081142

Apostolopoulou-Kalkavoura V, Gordeyeva K, Lavoine N, Bergström L (2018) Thermal conductivity of hygroscopic foams based on cellulose nanofibrils and a nonionic polyoxamer. Cellulose 25:1117–1126. https://doi.org/10.1007/s10570-017-1633-y

Apostolopoulou-Kalkavoura V, Hu S, Lavoine N, et al (2021) Humidity-Dependent Thermal Boundary Conductance Controls Heat Transport of Super-Insulating Nanofibrillar Foams Humidity-Dependent Thermal Boundary Conductance Controls Heat Transport of Super-Insulating Nanofibrillar Foams. Matter 4:1–14. https://doi.org/10.1016/j.matt.2020.11.007

Benítez AJ, Torres-Rendon J, Poutanen M, Walther A (2013) Humidity and multiscale structure govern mechanical properties and deformation modes in films of native cellulose nanofibrils. Biomacromolecules 14:4497–4506. https://doi.org/10.1021/bm401451m

Benítez AJ, Walther A (2017) Cellulose nanofibril nanopapers and bioinspired nanocomposites: A review to understand the mechanical property space. J Mater Chem A 5:16003–16024. https://doi.org/10.1039/c7ta02006f

Berthold J, Desbrières J, Rinaudo M, Salmén L (1994) Types of adsorbed water in relation to the ionic groups and their counter-ions for some cellulose derivatives. Polymer (Guildf). https://doi.org/10.1016/S0032-3861(05)80048-5

Candido RG, Gonçalves AR (2016) Synthesis of cellulose acetate and carboxymethylcellulose from sugarcane straw. Carbohydr Polym 152:679–686. https://doi.org/10.1016/j.carbpol.2016.07.071

Chen H, Hou A, Zheng C, et al (2020) Light- A nd Humidity-Responsive Chiral Nematic Photonic Crystal Films Based on Cellulose Nanocrystals. ACS Appl Mater Interfaces 12:24505–24511.

https://doi.org/10.1021/acsami.0c05139

Chen M, Coasne B, Guyer R, et al (2018) Role of hydrogen bonding in hysteresis observed in sorption-induced swelling of soft nanoporous polymers. Nat Commun 9:. https://doi.org/10.1038/s41467-018-05897-9

Committee S pulp paper and board testing (2002) Total acidic group content. Scand pulp, Pap board Test Comm 1–4

Cosgrove DJ (2005) Growth of the plant cell wall. Nat Rev Mol Cell Biol 6:850–861. https://doi.org/10.1038/nrm1746

Eyley S, Thielemans W (2014) Surface modification of cellulose nanocrystals. Nanoscale 6:7764–7779. https://doi.org/10.1039/c4nr01756k

Garg M, Linares M, Zozoulenko I (2020) Theoretical Rationalization of Self-Assembly of Cellulose Nanocrystals: Effect of Surface Modifications and Counterions. Biomacromolecules. https://doi.org/10.1021/acs.biomac.0c00469

Guo X, Liu L, Hu Y, Wu Y (2018) Water vapor sorption properties of TEMPO oxidized and sulfuric acid treated cellulose nanocrystal films. Carbohydr Polym 197:524–530. https://doi.org/10.1016/j.carbpol.2018.06.027

Hamad WY (2017) Cellulose Nanocrystals: Properties, Production and Applications. John Wiley & Sons, Ltd, Chichester, UK

Hanwell MD, Curtis DE, Lonie DC, et al (2012) Avogadro: an advanced semantic chemical editor, visualization, and analysis platform. J Cheminform 4:17. https://doi.org/10.1186/1758-2946-4-17

Haslach HW (2000) Moisture and rate-dependent mechanical properties of paper: a review. Mech Time-Dependent Mater 4:169–210. https://doi.org/10.1023/A:1009833415827

Kaldéus T, Larsson PT, Boujemaoui A, Malmström E (2018) One-pot preparation of bi-functional cellulose nanofibrils. Cellulose 25:7031–7042. https://doi.org/10.1007/s10570-018-2066-y

Klemm D, Kramer F, Moritz S, et al (2011) Nanocelluloses: A new family of nature-based materials. Angew Chemie - Int Ed 50:5438–5466. https://doi.org/10.1002/anie.201001273

Kontturi E, Spirk S (2019) Ultrathin films of cellulose: A materials perspective. Front Chem 7:1–18. https://doi.org/10.3389/fchem.2019.00488

Kulasinski K (2016) Effects of water adsorption in hydrophilic polymers. Polym Sci Res Adv Pract Appl Educ Asp 217–223

Kulasinski K, Guyer R, Derome D, Carmeliet J (2015) Water Adsorption in Wood Microfibril-Hemicellulose System: Role of the Crystalline-Amorphous Interface. Biomacromolecules 16:2972–2978. https://doi.org/10.1021/acs.biomac.5b00878

Langan P, Petridis L, O'Neill HM, et al (2014) Common processes drive the thermochemical pretreatment of lignocellulosic biomass. Green Chem 16:63–68. https://doi.org/10.1039/c3gc41962b

Lavoine N, Bergström L (2017) Nanocellulose-based foams and aerogels: processing, properties, and applications. J Mater Chem A 5:16105–16117. https://doi.org/10.1039/c7ta02807e

Li T, Li SX, Kong W, et al (2019) A nanofluidic ion regulation membrane with aligned cellulose nanofibers. Sci Adv 5:1–7. https://doi.org/10.1126/sciadv.aau4238

Liimatainen H, Visanko M, Sirviö J, et al (2013) Sulfonated cellulose nanofibrils obtained from wood pulp through regioselective oxidative bisulfite pre-treatment. Cellulose 20:741–749. https://doi.org/10.1007/s10570-013-9865-y

Mark P, Nilsson L (2001) Structure and dynamics of the TIP3P, SPC, and SPC/E water models at 298 K. J Phys Chem A 105:9954–9960. https://doi.org/10.1021/jp003020w

Mihranyan A, Llagostera AP, Karmhag R, et al (2004) Moisture sorption by cellulose powders of varying crystallinity. Int J Pharm 269:433–442. https://doi.org/10.1016/j.ijpharm.2003.09.030

Mokhothu TH, John MJ (2015) Review on hygroscopic aging of cellulose fibres and their biocomposites. Carbohydr Polym 131:337–354. https://doi.org/10.1016/j.carbpol.2015.06.027

Moon RJ, Martini A, Nairn J, et al (2011) Cellulose nanomaterials review: structure, properties and nanocomposites. Chem Soc Rev 40:3941. https://doi.org/10.1039/c0cs00108b

Munier P, Gordeyeva K, Bergström L, Fall AB (2016) Directional Freezing of Nanocellulose Dispersions Aligns the Rod-Like Particles and Produces Low-Density and Robust Particle Networks. Biomacromolecules 17:1875–1881. https://doi.org/10.1021/acs.biomac.6b00304

Niinivaara E, Faustini M, Tammelin T, Kontturi E (2015) Water Vapor Uptake of Ultrathin Films of Biologically Derived Nanocrystals: Quantitative Assessment with Quartz Crystal Microbalance and Spectroscopic Ellipsometry. Langmuir 31:12170–12176. https://doi.org/10.1021/acs.langmuir.5b01763

Paajanen A, Ceccherini S, Maloney T, Ketoja JA (2019) Chirality and bound water in the hierarchical cellulose structure. Cellulose 26:5877–5892. https://doi.org/10.1007/s10570-019-02525-7

Parker RM, Guidetti G, Williams CA, et al (2018) The Self-Assembly of Cellulose Nanocrystals: Hierarchical Design of Visual Appearance. Adv Mater 30:. https://doi.org/10.1002/adma.201704477

Phanthong P, Reubroycharoen P, Hao X, Xu G (2018) Nanocellulose: Extraction and application. Carbon Resour Convers 1:32–43. https://doi.org/10.1016/j.crcon.2018.05.004

Picheth GF, Pirich CL, Sierakowski MR, et al (2017) Bacterial cellulose in biomedical applications: A review. Int J Biol Macromol 104:97–106. https://doi.org/10.1016/j.ijbiomac.2017.05.171

Pinheiro M, Martin RL, Rycroft CH, et al (2013) Characterization and comparison of pore landscapes in crystalline porous materials. J Mol Graph Model 44:208–219. https://doi.org/10.1016/j.jmgm.2013.05.007

Plimpton S (1995) Fast Parallel Algorithms for Short – Range Molecular Dynamics. 117:1–42

Saito T, Isogai A (2004) TEMPO-mediated oxidation of native cellulose. The effect of oxidation conditions on chemical and crystal structures of the water-insoluble fractions. Biomacromolecules 5:1983–1989. https://doi.org/10.1021/bm0497769

Saito T, Isogai A (2006) Introduction of aldehyde groups on surfaces of native cellulose fibers by TEMPO-mediated oxidation. Colloids Surfaces A Physicochem Eng Asp 289:219–225. https://doi.org/10.1016/j.colsurfa.2006.04.038

Schrödinger (2018) Maestro | Schrödinger. Schrödinger Release 2018-1

Segal L, Creely JJ, Martin AE, Conrad CM (1959) An Empirical Method for Estimating the Degree of Crystallinity of Native Cellulose Using the X-Ray Diffractometer. Text Res J 29:786–794. https://doi.org/10.1177/004051755902901003

Shrestha S, Diaz JA, Ghanbari S, Youngblood JP (2017) Hygroscopic Swelling Determination of Cellulose Nanocrystal (CNC) Films by Polarized Light Microscopy Digital Image Correlation. Biomacromolecules 18:1482–1490. https://doi.org/10.1021/acs.biomac.7b00026

Solin K, Borghei M, Sel O, et al (2020) Electrically Conductive Thin Films Based on Nanofibrillated Cellulose: Interactions with Water and Applications in Humidity Sensing. ACS Appl Mater Interfaces. https://doi.org/10.1021/acsami.0c09997

Tanaka R, Saito T, Hondo H, Isogai A (2015) Influence of flexibility and dimensions of nanocelluloses on the flow properties of their aqueous dispersions. Biomacromolecules 16:2127–2131. https://doi.org/10.1021/acs.biomac.5b00539

Thomas B, Raj MC, Athira BK, et al (2018) Nanocellulose, a Versatile Green Platform: From Biosources to Materials and Their Applications. Chem. Rev. 118:11575–11625

Trache D, Hussin MH, Hui Chuin CT, et al (2016) Microcrystalline cellulose: Isolation, characterization and bio-composites application—A review. Int J Biol Macromol 93:789–804. https://doi.org/10.1016/j.ijbiomac.2016.09.056

Wågberg L, Decher G, Norgren M, et al (2008) The build-up of polyelectrolyte multilayers of microfibrillated cellulose and cationic polyelectrolytes. Langmuir 24:784–795. https://doi.org/10.1021/la702481v

Wicklein B, Kocjan A, Salazar-Alvarez G, et al (2015) Thermally insulating and fire-retardant lightweight anisotropic foams based on nanocellulose and graphene oxide. Nat Nanotechnol 10:277–283. https://doi.org/10.1038/nnano.2014.248

Figures

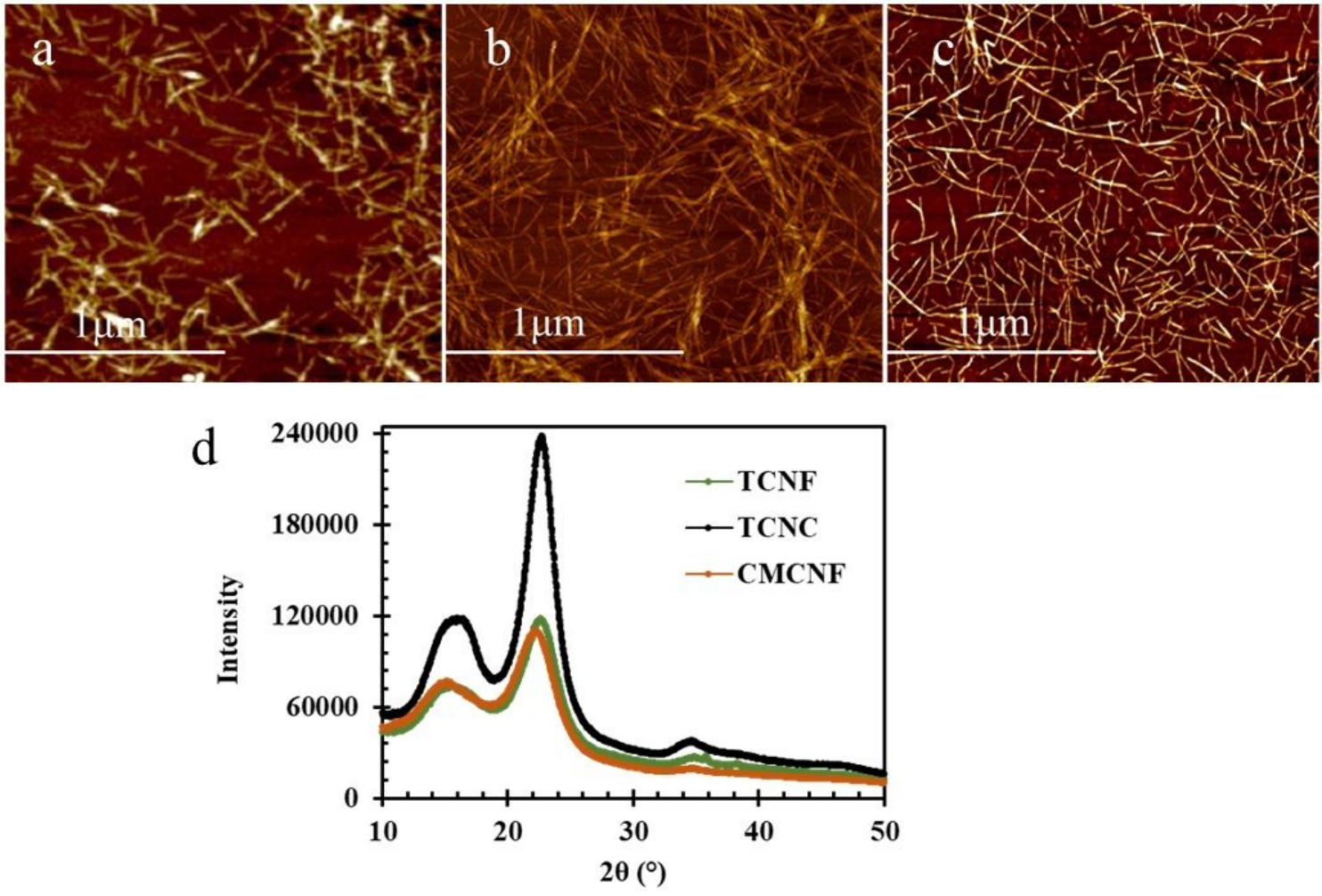

Figure 1

AFM image of (A) TCNF, (B) TCNC, and (C) CMCNF. (D) X-ray diffraction spectra for a TCNC (black), TCNF (green) and CMCNF (orange) foams used for determining the crystallinity index.

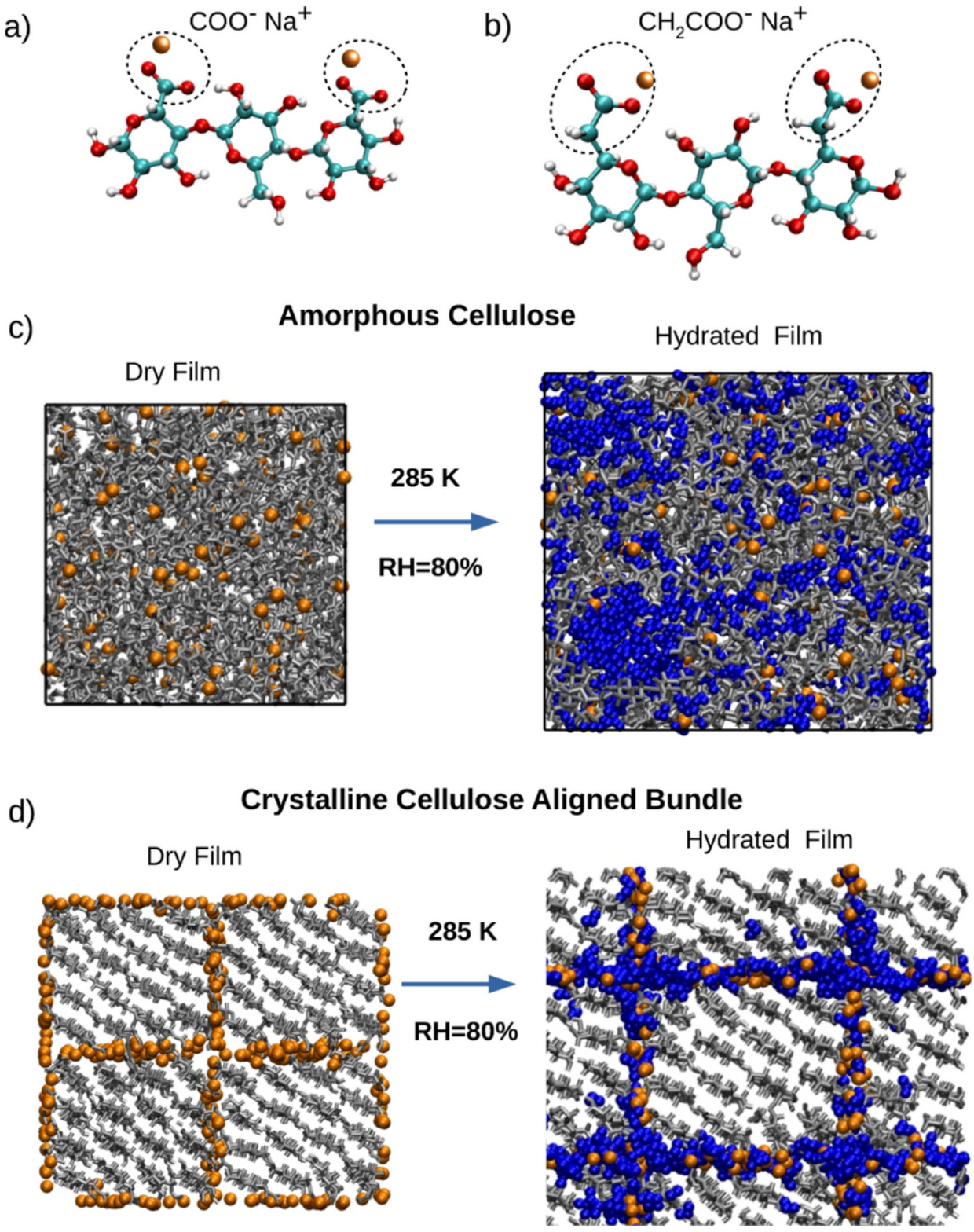

Figure 2

Cellulose chains functionalized via: (a) carboxylate groups (TEMPO), (b) Carboxymethylated groups and neutralized by Na+ counterion (in orange), (c) Amorphous cellulose film at initial dry state and final hydrated state when subjected to 80% RH and temperature of 285 K, (d) Array of four cellulose nanocrystals arranged in bundle at initial dry state and hydrated state when subjected to 80% RH at 285 K. The cellulose chains and water molecules are shown in grey and blue color respectively.

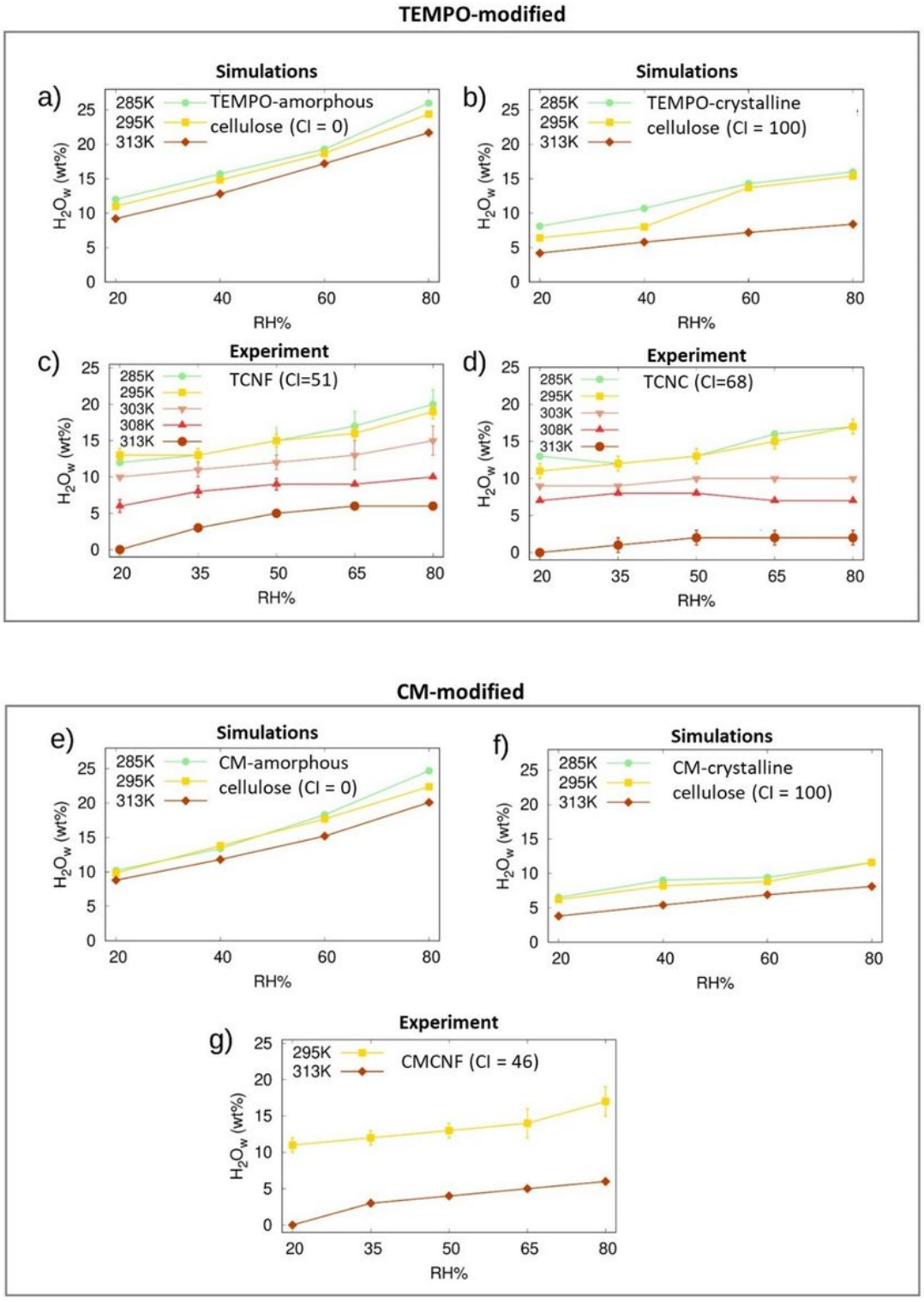

Figure 3

Simulated and experimental values of moisture uptake (weight percent on dry basis) as a function of relative humidity and at different temperatures for: a) TEMPO-modified amorphous cellulose films (simulations); b) bundles of TEMPO-modified 100% crystalline CNC (simulations); c) TCNF foams (experimental); d) TCNC foams (experimental); e) carboxymethylated amorphous cellulose films (simulations); f) bundles of carboxymethylated CNC (simulations); g) CMCNF foams (experimental).

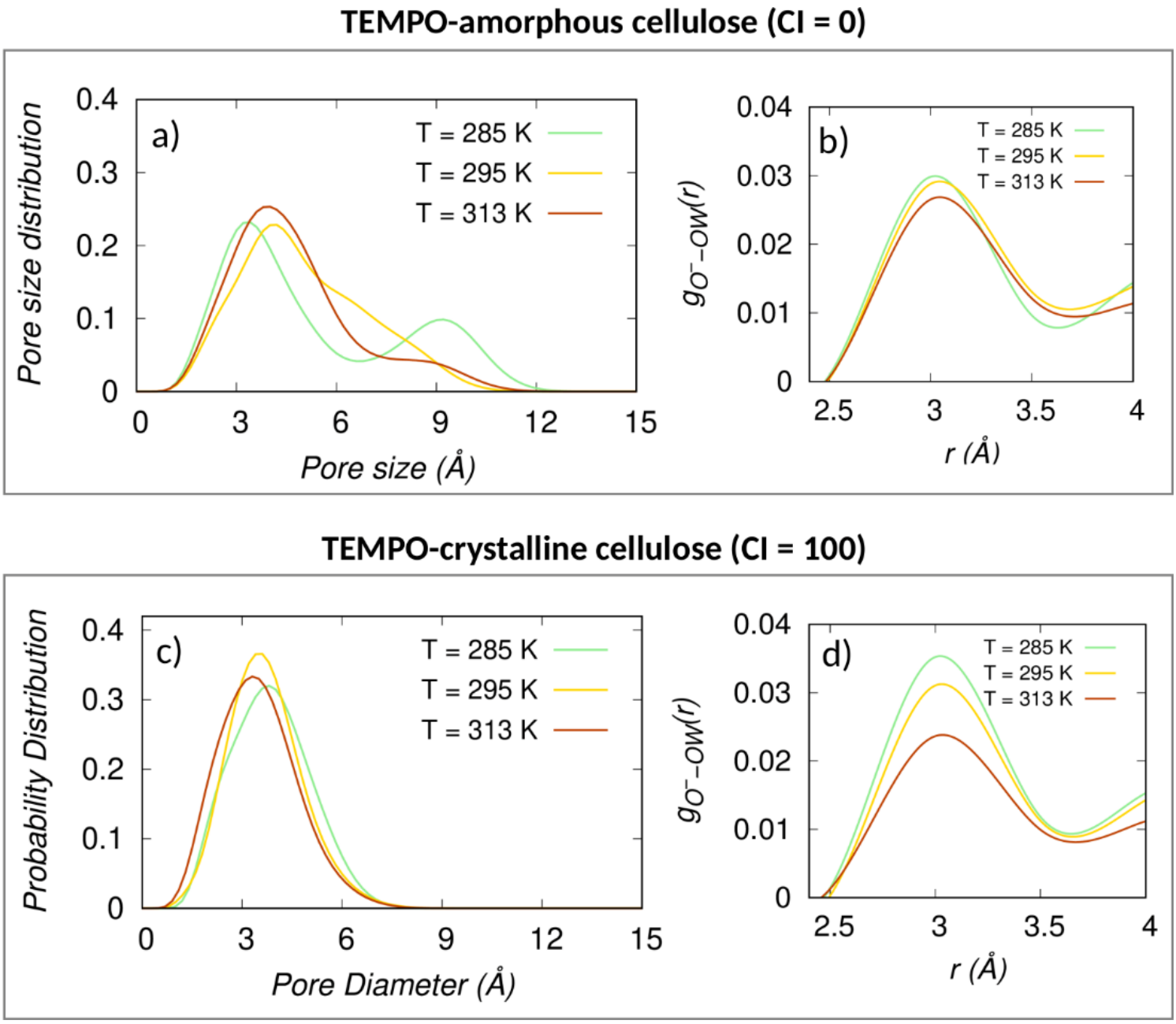

Figure 4

(a) and (c) Pore size distribution as a function of pore size, and (b) and (c) the radial pair distribution gO–OW(r) between the oxygen (O-) of carboxyl group and oxygen (OW) of water for different temperatures T=285K, 295K, 313K. Upper and lower panels correspond to respectively TEMPO-amorphous cellulose and TEMPO-crystalline cellulose. The relative humidity is 80%.

Supplementary Files

This is a list of supplementary files associated with this preprint. Click to download.

- SIMoistureuptakesubmittedCellulose.docx